

X-RAY IGM IN THE LOCAL GROUP

Andrew Rasmussen, Steven M. Kahn and Frits Paerels

Columbia University

arasmus@astro.columbia.edu

Abstract Recent observations with the dispersive X-ray spectrometers aboard *Chandra* and *Newton Observatory* have begun to probe the properties of the X-ray intergalactic medium (IGM) at small redshifts. Using large quantities (~ 950 ksec) of spectroscopic data acquired using the Reflection Grating Spectrometer (RGS) aboard *Newton Observatory*, we investigated the intervening material toward three low redshift, high Galactic latitude Active Galactic Nuclei (AGNs) with nominally featureless spectra: Mrk 421, PKS 2155–304 and 3C 273. Each spectrum provides clear evidence for what appears to be a local ($z \sim 0$), highly ionized absorbing medium betrayed by the O VII 1s–2p resonance transition feature seen at 21.6Å (NovII $\sim 10^{16}$ cm $^{-2}$). Measurements are also made for the Ly α transition of the adjacent ionization state, (O VIII; 18.97Å), which potentially constrains the absorber's temperature. Finally, in a collisional equilibrium approximation, upper limits to diffuse emission intensities place upper limits on the electron density ($n_e < 2 \times 10^{-4}$ cm $^{-3}$), lower limits on the scale length of the absorber ($L > 140$ kpc) and lower limits on its mass ($M > 5 \times 10^{10}$ M $_{\odot}$). Limits on the absorber's scale length and its velocity distribution lead us to identify it with the Local Group. Having detected the hot gas in our Local Group in absorption, it should be feasible to detect also the extended structure of other low-mass, spiral-dominated groups of galaxies in absorption, with spectra of similar quality.

1. Introduction

That local intergalactic space could harbor substantial amounts of hot, highly ionized gas, either as an extended halo surrounding the Galaxy, or as an extended medium pervading the Local Group, was first suggested by Spitzer (1956) and by Kahn and Woltjer (1959). Such a medium would have a characteristic temperature of order the virial temperature, estimated to be on the order of $T \sim 2 - 3 \times 10^6$ K, and be of very low density, $n_e \sim 10^{-4}$ cm $^{-3}$ (Maloney and Bland-Hawthorn, 1999). Its emission, mainly soft thermal line emission from highly ion-

ized metals and weak thermal bremsstrahlung, would be very faint and extremely difficult to detect, and searches for diffuse hot gas have relied on detecting its absorption lines in bright background continuum sources. Detailed studies of Li-like C and O absorption lines in the UV in background quasar spectra have indeed revealed the presence of gas in the Galactic Halo (*e.g.*, Savage et al., 2000) and, more recently, beyond (*e.g.*, Tripp et al., 2000).

Intergalactic X-ray absorption spectroscopy has long been recognized as having the potential of revealing more highly ionized gas, but the required spectroscopic sensitivity has only recently become available with the diffraction grating spectrometers on *Chandra* and *XMM-Newton*. The first detection of resonance absorption lines from H- and He-like oxygen and neon, in a spectrum of the bright BL Lac object PKS 2155–304 with the *Chandra* Low Energy Transmission Grating Spectrometer, was recently reported (Nicastro et al., 2002). Here we report on multiple detections of the $1s - 2p$ resonance lines in H- and He-like oxygen in deep spectra of PKS 2155–304, Mrk 421, and 3C 273, obtained with the Reflection Grating Spectrometer (RGS) on *XMM-Newton*. The O VII lines appear at zero redshift, with characteristic equivalent widths of 15 mÅ; the O VII line in Mrk 421 appears marginally resolved, with a characteristic velocity width of 300 km s^{-1} . We will argue that the bulk of the absorption in these lines arises in an extended low density medium in near collisional equilibrium, well outside our Galaxy, which is likely the long sought-for intragroup medium of the Local Group.

2. Data and Analysis

Weak X-ray absorption features are detectable only when spectra of sufficient photon statistics were acquired with the grating spectrometers, and when various systematic effects of the detectors to the histogrammed data sets can be minimized. To prepare such spectra, we combined the available spectroscopic data toward the three high latitude AGNs from a combination of calibration, performance verification, and guaranteed time observation data sets available to the *XMM-Newton* RGS team. Using all of the available datasets, the effective exposure times added up to 412, 274 and 265 ksec for 3C 273, Mrk 421 and PKS 2155–304, respectively. Custom software was used to operate on the observation data file (ODF) in each case, to produce spectra aligned to the same dataspace grid. The custom software is identical in function to, and shares a common origin with, the RGS branch of the science analysis subsystem (SAS), except that it allowed a flexible means by which to reduce systematic effects to the data. Because there is a residual pointing

uncertainty on the order of 2" for the analysis at this time, the reported velocities should be accompanied by systematic wavelength uncertainties of order of $\pm 5\text{m}\text{\AA}$, or 70 km s^{-1} for a line close to 20\AA . The relative error in wavelength between two line measurements from the same observation is much lower.

Because AGNs typically have variable spectra, the continuum spectrum from each observation was fit separately, and the ratio spectra (“data:folded model”) were counts-weighted to yield a final absorption spectrum toward each of the AGNs. These are displayed in Figure 1, uncorrected for instrumental and interstellar absorption features. For comparison, the spectrum of Capella is displayed on the top panel, which can be used to identify the locations of strong transitions in the rest frame. Each AGN spectrum exhibits a clear signature of intervening O VII by the $1s-2p$ He α transition at 21.60\AA . Hints of the O VIII $1s-2p$ Ly α and O VII $1s-3p$ He β transitions are also seen at 18.63 and 18.97\AA , respectively. We fit the absorption line profiles in the data within XSPEC using a Voigt model folded through the instrumental redistribution matrices.

3. Results

A quantitative summary of the absorption features measured is given in Table 1. The spectrum toward Mrk 421 had superior statistics, and provided detections in four transitions: $1s-2p$ in O VIII, O VII, Ne IX and C VI. Of these, the strongest absorption feature (O VII) appears to be marginally resolved, and yields an ionic velocity dispersion V_{turb} between 200 and 560 km s^{-1} , based on 90% confidence levels and, in a Gaussian approximation to the line-of-sight velocity distribution characterized by σ_v , $V_{\text{turb}} = \sqrt{2}\sigma_v$. In most cases, fitting the absorption features works significantly better when a line broadening mechanism beyond the thermal velocity distribution is included.

While the measured line equivalent widths (from Voigt profile fitting) are given in Table 1, estimating the corresponding ionic column densities (N_i) requires an assumption of the velocity distribution. The rightmost column gives a conservative lower limit to the true column density for each ion species measured: We use the 90% lower limit to the equivalent width of the feature, and then tabulate the corresponding ionic column density in the unsaturated limit. The true column density, however, can depend strongly on the true velocity distribution for a given measured equivalent width. For example, for both Mrk 421 and 3C 273, the inferred N_i values increase by a factor of 2 when the velocity dispersion parameter is reduced to 100 km s^{-1} from $\sim 300\text{ km s}^{-1}$, where the fits provide marginally better χ^2 values.

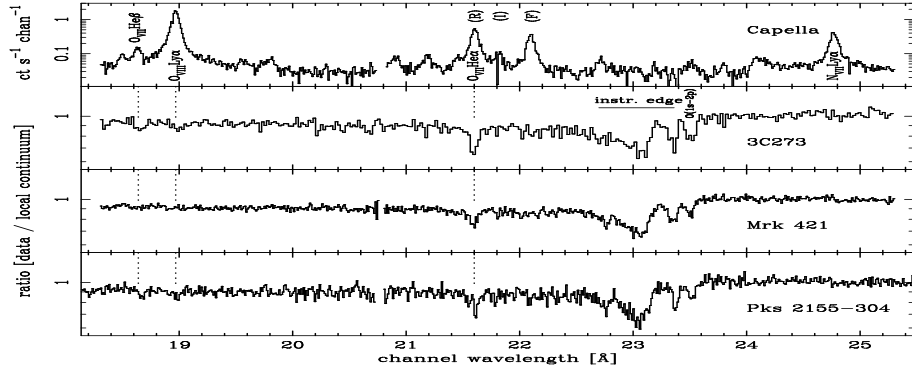


Figure 1 A comparison of the three AGN spectra used in this study, displayed in the range 18.3 to 25.3 Å.

Table 1. Absorption line fitting results.

Target	EW ^a (mÅ)	Significance	Centroid min	Velocity ^a max	V _{turb} ^a min	V _{turb} ^a max	N _i (min) ^b 10 ¹⁶ cm ⁻²
O VII He α 1s – 2p (λ 21.602)							
3C 273	26.3 ^{+4.5} _{-4.5}	10.2 σ	-190	+46	0	638	0.76
Mrk 421	15.4 ^{+1.7} _{-1.7}	15.7 σ	-254	-98	203	563	0.48
PKS 2155	16.3 ^{+3.3} _{-3.3}	8.1 σ	-182	+233	0	963	0.45
O VIII Ly α 1s – 2p (λ 18.970)							
3C 273	11.7 ^{+3.6} _{-3.7}	5.6 σ	-47	+711	122	1020	0.60
Mrk 421	4.3 ^{+1.0} _{-1.1}	6.8 σ	-648	-366	0	387	0.24
PKS 2155	9.0 ^{+2.6} _{-2.7}	5.7 σ	-427	+95	415	1555	0.48
C VI Ly α 1s – 2p (λ 33.734)							
3C 273	12.9 ^{+4.1} _{-4.3}	5.0 σ	-133	+111	0	311	0.21
Mrk 421	3.5 ^{+1.9} _{-1.6}	3.6 σ	-164	+132	0	292	0.05
PKS 2155	NA	NA	NA	NA	NA	NA	NA
Ne IX He α 1s – 2p (λ 13.447)							
3C 273	14.3 ^{+17.7} _{-14.3}	2.3 σ	NA	NA	NA	NA	NA
Mrk 421	3.0 ^{+1.2} _{-1.3}	3.7 σ	-747	1138	NA	NA	0.15
PKS 2155	0.0 ^{+2.8} _{-0.0}	0.0 σ	NA	NA	NA	NA	NA

^aRanges and errors given are 90% confidence limits. Velocities are given in km s⁻¹. Absolute velocity uncertainties due to (systematic) pointing uncertainties are not reflected in these confidence intervals, and are expected to be on the order of $\Delta v \sim 70 \times (\lambda/20)^{-1}$ km s⁻¹.

^bMinimum ion column density is computed by converting the EW lower limit in the unsaturated approximation: $N_i(\min) \equiv \text{EW}_{\min} \times (f \pi e^2 / mc^2)^{-1} \lambda^{-2}$.

Another fact to note in the fitting results is that the O VII and O VIII feature positions do not match up in their systemic velocities and velocity widths. While there are in most cases systemic velocities and V_{turb} that satisfy the 90% limits for both lines for a given AGN, the differences seen in them evoke a possible situation where the absorption features may probe different velocity components, and therefore different phases of the intervening gas. When a fit was performed simultaneously to the O VII and O VIII features with velocity parameters tied, a lower equivalent width and column density was derived for the O VIII feature, because the fit was driven by details of the O VII feature profile – additional velocity components are then required to fit the excess O VIII. From the column density ratios for O VIII to O VII derived this way (0.3 for Mrk 421 to 0.8 for PKS 2155) we estimate the electron temperatures by assuming collisional equilibrium and that the O VII and O VIII occupy the same volume. The electron temperature range, according to this assumption, is $2 - 5 \times 10^6$ K, which brackets the 1σ confidences for each of the targets.

Collisional excitation and emission from the same medium may be estimated from the ROSAT all-sky survey toward these lines of sight. Alternatively, a better estimate of the emission line contribution to the diffuse X-ray background is provided by results of a recent sounding rocket experiment (X-ray Quantum Calorimeter, McCammon et al., 2002). Their analysis estimated that the Oxygen line fluxes (for $z < 0.01$) together account for 32% of the R4 band count rates. However, because the calorimeter provided individual line fluxes (*e.g.*, $dI/d\Omega = 4.8 \pm 0.8 \text{ phot s}^{-1} \text{ cm}^{-2} \text{ sr}^{-1}$ in the O VII triplet) electron densities and lengths through the emitter-absorber may be estimated. In the approximation that the medium has a uniform density and temperature out to some distance L , the ionic column density should be $N_i = A_O f_i n_p L$ and the diffuse emission intensity $dI/d\Omega = (1/4\pi) A_O f_i n_p n_e \gamma(T) L$ where A_O , f_i and $\gamma(T)$ are the elemental abundance, ionic fraction and collisional rate coefficient for the transition, respectively. Since the ion column density is formally a lower limit and the surface brightness is an upper limit to true diffuse contribution, an upper limit to the electron density n_e can be estimated in a way that is independent of oxygen abundance. Then, by assuming an oxygen abundance and ionic fraction, a lower limit to the length L is estimated. Figure 2 shows a graphical solution to the emitter-absorber for a range of temperatures and some assumptions ($A_O \sim 0.3 A_\odot$, $f_i \sim 0.5$, $dI/d\Omega \sim 4 \text{ phot s}^{-1} \text{ cm}^{-2} \text{ sr}^{-1}$ and $N_i \sim 10^{16} \text{ cm}^{-2}$). From the temperature T inferred from the column density ratios, the electron density estimate yields $n_e < 2 \times 10^{-4} \text{ cm}^{-3}$ and a length scale $L > 140 \text{ kpc} (A_O/0.3 A_\odot)^{-1}$, ~ 40 times larger (and

more tenuous) than the O VI absorbing Galactic halo (Savage et al., 2000).

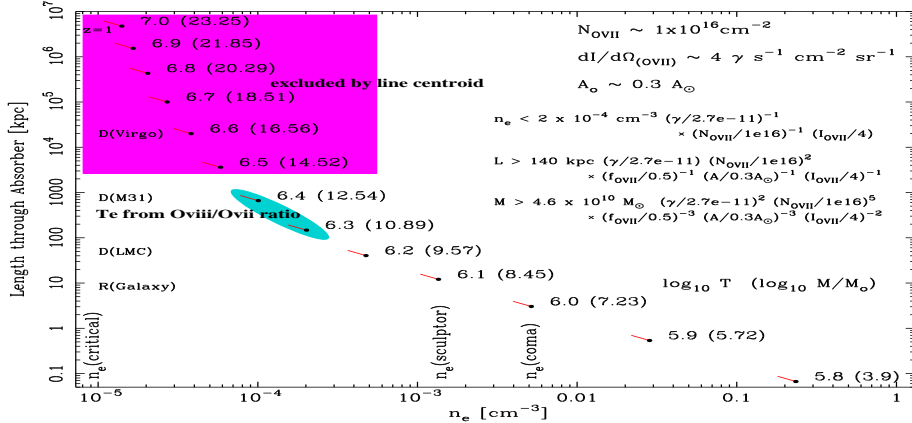


Figure 2 Solutions to the emitter-absorber problem for a uniform medium under CIE conditions. For each temperature, the black dot represents the solution for n_e and L , while the red line is along the column density constraint, pointing away from the upper limit for n_e .

4. Conclusions

The results of this initial survey of $z \sim 0$ absorption by highly ionized gas in the high Galactic latitude pointings provide a picture of IGM in the local group that can be tested toward other galaxies in poor groups. With impact parameters on the order of 100 kpc from spiral galaxies such as our own, the spectra of more distant AGNs should contain absorption features with characteristic column densities of $N_i \sim 10^{16} \text{ cm}^{-2}$ in O VII. Such extended, tenuous halos or intragroup gas should consequently be accompanied by a diffuse glow, that would only double the local surface brightness of the X-ray background's diffuse and line-rich component on the 100 kpc scale, and would be very difficult to detect.

References

Kahn, F. D. and Woltjer, L. (1959). *ApJ*, 130:705–+.
 Maloney, P. R. and Bland-Hawthorn, J. (1999). *ApJ*, 522:L81–L84.
 McCammon, D. et al. (2002). *ApJ*, 576:188–203.
 Nicastro, F. et al. (2002). *ApJ*, 573:157–167.
 Savage, B. D. et al. (2000). *ApJ*, 538:L27–L30.
 Spitzer, L. J. (1956). *ApJ*, 124:20–+.
 Tripp, T. M., Savage, B. D., and Jenkins, E. B. (2000). *ApJ*, 534:L1–L5.